ICAS 2021 SHANG HAI
International Council of the Aeronautical Sciences
32nd Congress of the International Council of the Aeronautical Sciences
September 6-10, 2021
Pudong Shangri-La, Shanghai, China

Mechanism Design and Aerodynamic Research of Retractable Folding Flapping Wing

Yuanbo Li [1], Wenqing Yang [1], Ang Chen [1] & Rui Zhang [1]

[1] School of Aeronautics, Northwestern Polytechnical University, Xi'an 710072, China

Abstract

Inspired by the physiological structure and retractable characteristics of bat wings, a folding wing mechanism is designed and numerically investigated. The humerus, radius and phalanges in the bat wing skeleton are extracted first, and the connecting rod is used to simulate them, and then the auxiliary connecting rod is added, so that the whole connecting rod mechanism could imitate the folding of the bat wing to a higher degree. Secondly, a special locking mechanism and driving mechanism are designed to realize the coupling of folding and flapping motion of the whole mechanism. The CATIA motion simulation module is used as the platform to analyze the kinematics of the designed mechanism model. The simulation results are in line with the expected design objectives.

In order to study the effects of wingspan contraction on lift and thrust, Computational Fluid Dynamics (CFD) simulation is carried out on the simplified rectangular flat wing. Comparing the lift and thrust of the wing with and without spanwise contraction, it is found that the wing spanwise contraction can reduce the negative lift during the upstroke due to the reduction of area, thereby increasing the averaged lift, but at the same time the thrust is also reduced.

Keywords: retractable wing, spanwise contraction, mechanism, aerodynamic performance

1. Introduction

Flapping wing aircraft is a kind of innovative aircraft which imitates the flapping wing flying creatures in nature, and its flying principle comes completely from the natural flying creatures. At present, many kinds of flapping wing aircraft have been developed by various countries in the world, which are mainly based on imitating birds or insects. However, there are relatively less researches on the design of bat-like aircraft. The California Institute of Technology developed a "Micro Bat" aircraft [1,2], using titanium alloy metal as the wing skeleton and parylene-C as the wing membrane. Through a lightweight transmission mechanism, the rotation of the micro motor is converted into the flapping of the wings. The first prototype successfully flew for 9 seconds. Chung [3,4] used mathematical formulas and theoretical control models to describe the three-dimensional (3D) movement law of bat wings, and designed a 10-DOF mechanism to simulate the movement law of bat wings. However, its shape, structure and function are still quite different from that of real bats. Breuer [5] designed a bat wing that can flap, using ABS plastic for the skeleton and latex for the wing membrane. Bahlman [6,7] designed and made a 3-DOF robotic wing, and studied the inertial characteristics and wing folding in the wind tunnel. The results showed that the inertial power consumption and inertial force in the movement of bat wings could not be ignored, and wing folding was beneficial to improve aerodynamic force. He also measured the influence of flapping frequency, flapping amplitude and wing folding on the aerodynamic force and mechanical power consumption of the robotic wing. The results showed that the influence of these parameters on the aerodynamic force and mechanical power consumption was not different. Chen [8] designed a robotic wing with a wing size three times that of a bat, using metal material to make a wing skeleton, and the maximum flapping frequency is 4Hz. Koekkoek [9] designed a robotic wing resembling a long-nosed bat. The wing membrane was made of latex, and the wing skeleton was made of carbon epoxy resin, which could realize flapping, twisting and folding

movements of the wing. Colorado [10-14] used shape memory alloy materials to make driving muscles and flexible joints, and used plastic to make wing skeletons and wing membranes, and developed a bat-like flapping wing platform and conducted experiments. The results show that the wings contract rapidly in the upstroke, and the slow deployment in the downstroke is beneficial to the wings to increase lift and reduce drag.

Due to the difficulty of developing bat-like aircraft, researchers have focused on the structure of bat-like mechanical wings, and designed a number of bat-like mechanical wings. However, to develop efficient bat-like mechanical wings, it is still necessary to design reasonable mechanisms and add appropriate degrees of freedom, so that the appearance and movement of the mechanical wings can be consistent with the real bats. Based on the observation and summary of the folding characteristics of bat wings in nature, this paper analyzes the structural characteristics and movement forms of wing expansion and contraction, extracts the key positions of wing folding, and designs a bat-like retractable folding mechanism. It fully expands its wings on the downstroke, and folds the wings first and then expands to the original length on the upstroke. This mechanism is simplified into a flat plate model, and the FLUENT software is used to numerically simulate the folding motion of the flat plate. The results show that the flat plate with folding motion has better aerodynamic performance.

2. Study on the physiological structure and retractable characteristics of bat wings

Bats are the only mammals in the world that can fly. Its wings are mainly composed of skeletons, joints, and wing membranes. The skeleton structure is similar to that of a human arm. As shown in Figure 1, the bat wing skeleton mainly includes the humerus, radius, and phalanx. Compared to human arms, bats have longer wing skeletons, longer phalanx, and relatively larger wings. The main joints of bats include the shoulder joint between the bat body and the humerus, the elbow joint between the humerus and the radius, the wrist joint between the radius and the phalanx, and the knuckle inside the phalanx.

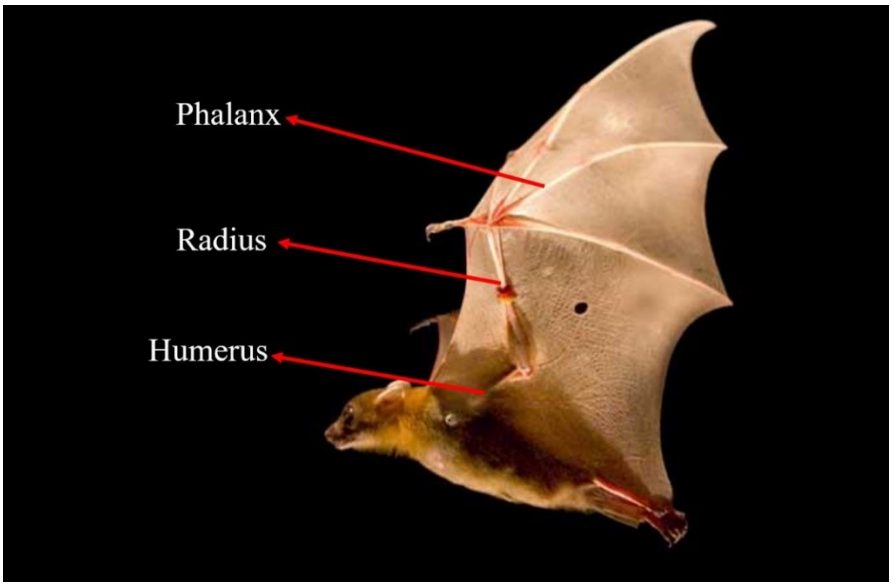

Figure 1 – Bat wing skeleton structure.

The spanwise folding of bat wings mainly relies on the coordination of the humerus, radius and phalanges inside the bat wing. During fast flight, bats fly in a similar way to birds, but at low speeds, these two flying creatures fly differently. Birds spread their feathers to reduce drag on the upstroke, while bats fold their wings to reduce the area on the upstroke to reduce drag.

3. Design of bat-like retractable folding wing mechanism

3.1 2D design of bat-like folding mechanism

Through careful observation of the physiological structure of bat wings, a bat-like folding mechanism is proposed. The two-dimensional (2D) schematic diagram of the mechanism is shown in Figure 2. The connecting rods AG, GH and HK imitate the humerus, radius and phalanx in the bat wing skeleton respectively. These three connecting rods are the main rods of the entire folding mechanism, and the remaining connecting rods are auxiliary connecting rods. This folding mechanism can be divided into three parts: inner wing section, middle wing section and outer wing section. The four-bar linkage ABCD and connecting rod AG, EF constitute the inner wing section. The four-bar linkage GHIJ and connecting rod HB constitute the middle wing section. The connecting rod IK constitutes the outer wing section. The whole mechanism is composed of several connecting rods, rotating pairs, and sliding pairs, forming a complex multi-link mechanism.

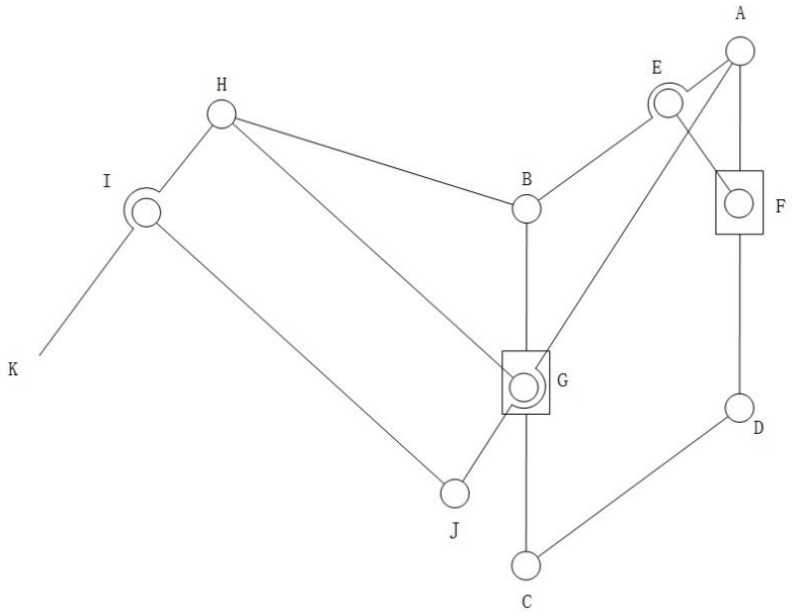

Figure 2 – Schematic diagram of bat-like folding mechanism.

For the inner wing section, the connecting rod AD is fixed to the frame, and the four-bar linkage ABCD is a parallelogram four-bar linkage mechanism. The drive mechanism (not shown in the figure) drives the slider F to reciprocate back and forth to realize the expansion and folding of the four-bar linkage ABCD.

For the middle wing section, the four-bar linkage GHIJ is also a parallelogram four-bar linkage. Due to the unfolding and folding of the inner wing section, the position of the node B is constantly changing, and the four-bar linkage GHIJ is driven to unfold and fold through the change of the position of the connecting rod BH and the action of the connecting rod AJ. The connecting rod GJ is a part of the connecting rod AG that extends outward, and the entire connecting rod AJ couples the inner wing section and the middle wing section together. The connecting rods AG and HG are hinged on the slider G. When the entire mechanism is unfolded, the slider G slides to the node C along the track BC, and slides to the node B when folded.

For the outer wing section, since the connecting rod IK is a part of the connecting rod HI extending outward, the outer wing section is retracted passively by the middle wing section.

The theoretical diagrams of the entire bat-like folding mechanism when fully folded and fully unfolded are shown in Figure 3 and Figure 4.

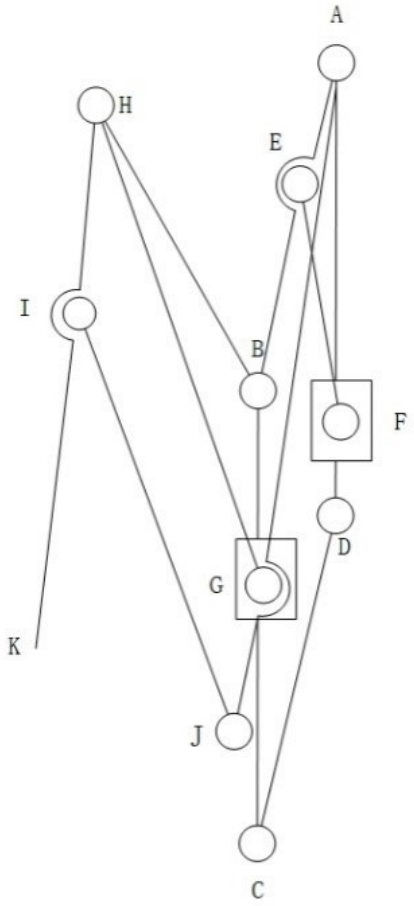

Figure 3 – Schematic diagram of fully folded bat-like folding mechanism.

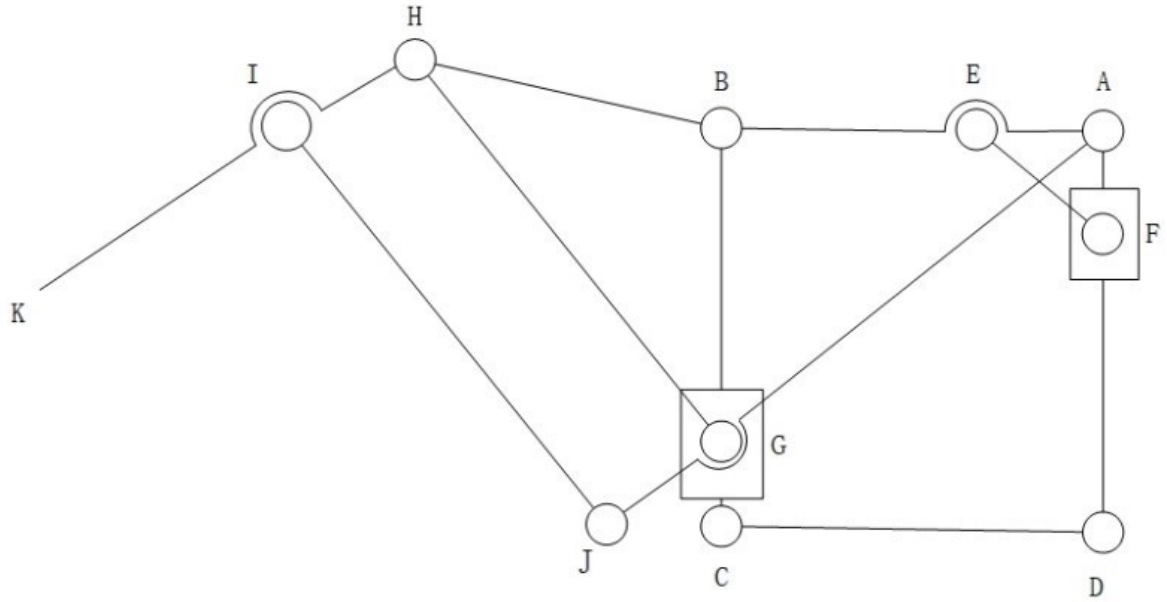

Figure 4 – Schematic diagram of fully expanded bat-like folding mechanism.

The 3D model of the folding mechanism is drawn through the CATIA modeling software, as shown in Figure 5.

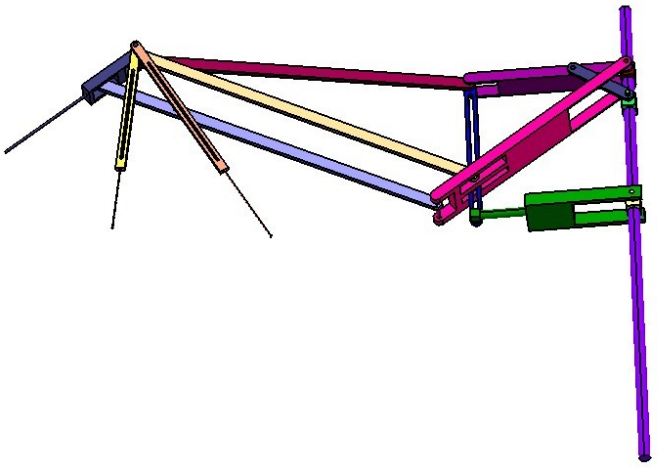

Figure 5 – 3D model of bat-like folding mechanism.

3.2 Locking mechanism design

The bat wings are fully expanded during the downstroke, while the bat wings will contract during the upstroke. Therefore, it is necessary to design a locking mechanism that can achieve the following functions:

1) When the entire mechanism is in the downstroke, the locking mechanism locks the flapping wing to maximize its area.

2) When the entire mechanism is in the upstroke, the locking mechanism is unlocked so that the flapping wings are first folded and then fully unfolded.

Such a locking mechanism is proposed, as shown in Figure 6. The mechanism is composed of an inner sliding rod, an outer sliding rod and a pin shaft. The inner and outer sliding rods are sleeved together, and the pin shaft passes through the internal common track of the two sliding rods.

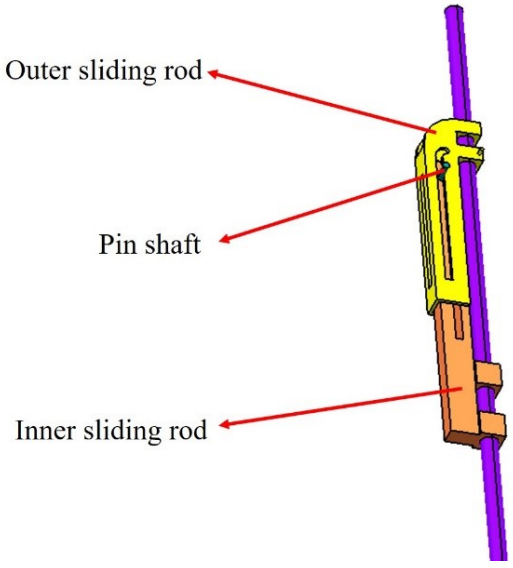

Figure 6 – Locking mechanism.

The partial enlarged top view is shown in Figure 7. In this top view, the two black lines respectively represent the center lines of the inner rails of the inner and outer slide rods, and the square black dot represents the center of the upper surface of the cylindrical pin shaft. The parameters of the inner rail of the inner and outer slide rods are the same except that the upper end of the rail is bent in the opposite direction and the total length of the rail is different. The pin shaft can be placed in the overlap

of the inner rails of the two slide rods. Both the inner and outer sliding rods can rotate around the right cylindrical fixed rod, but the inner sliding rod cannot move in translation along the fixed rod axis, and the outer sliding rod can move in translation along the fixed rod axis.

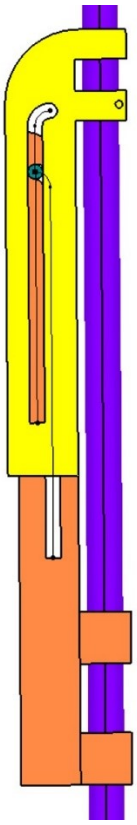

Figure 7 – Partial enlarged top view of locking mechanism.

The translation of the outer sliding rod along the axis of the fixed cylindrical rod on the right is divided into four phases, and it is assumed that the outer sliding rod is at the position shown in Figure 8 at the initial moment. At this time, the tangent point between the straight line of the inner rail center line of the outer slide rod and the 1/4 arc, the end point of the inner rail center line of the inner slide rod, and the center point of the upper surface of the cylindrical pin shaft are combined at one point in this top view.

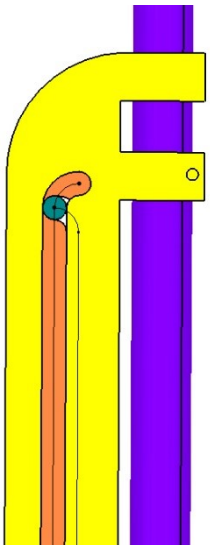

Figure 8 – The initial position of the outer slide rod in the locking mechanism.

1) Phase 1:

The outer slide rod translates forward from the initial position to the farthest position (the position shown in Figure 9). During this process, the cylindrical pin shaft is stuck in the arc track of the inner slide rod and cannot move under the action of the straight track of the outer slide rod, that is, it is locked in the inner slide rod track.

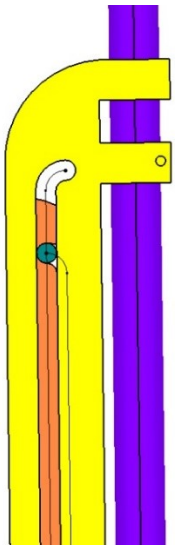

Figure 9 – The farthest forward position of the outer slide rod in the locking mechanism.

2) Phase 2:

The outer slide rod moves backward from the farthest position (position shown in Figure 9) to the initial position (position shown in Figure 8). In this process, the cylindrical pin shaft is also stuck in the arc track of the inner slide rod by the action of the straight track of the outer slide rod, that is, locked in the inner slide rod track.

3) Phase 3:

The outer slide rod continues to move backward to the farthest position (the position shown in Figure 10). During this process, under the joint action of the arc track of the outer slide rod and the inner slide rod, the cylindrical pin shaft will leave the arc track of the inner slide rod and slide into the straight track. After that, the cylindrical pin shaft is stuck in the arc track of the outer slide rod under the action of the straight track of the inner slide rod, and moves in translation with the translation of the outer slide rod.

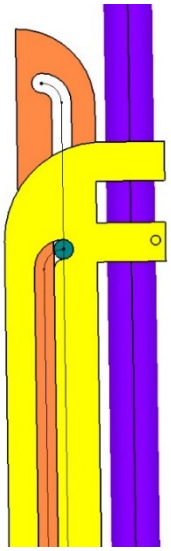

Figure 10 – The farthest backward position of the outer slide rod in the locking mechanism.

4) Phase 4:

The outer sliding rod moves from the farthest position of the backward translation (position shown in Figure 10) to drive the cylindrical pin shaft to move forward until the initial position (position shown in Figure 8). During this process, the cylindrical pin shaft is stuck in the arc track of the outer slide rod under the action of the straight track of the inner slide rod, and moves in translation with the translation of the outer slide rod.

In the four phases, the position of the cylindrical pin shaft in the first and second phases remains unchanged, and the position of the cylindrical pin shaft in the third and fourth phases moves in translation with the translation of the outer sliding rod. We can associate the downstroke of the bat wings with phases one and two, and the upstroke with phases three and four.

1) Downstroke of bat wings:

The outer slide rod in the locking mechanism translates forward from the initial position to the farthest position, and then translates backward from the farthest position to the initial position. Since the cylindrical pin shaft is locked and cannot move during this process, the folding mechanism can be locked to the fully unfolded state through the inability of the cylindrical pin shaft to move. Therefore, during the downstroke stage of the bat wings, the folding mechanism is always fully extended.

2) Upstroke of bat wings:

The outer sliding rod of the locking mechanism continues to move backward to the farthest position, and then from the farthest position to drive the cylindrical pin shaft to move forward to the initial position. During this process, the cylindrical pin shaft will leave the arc track of the inner slide rod and slide into the straight track, and be stuck in the arc track of the outer slide rod by the straight track of the inner slide rod, and move back and forth with the front and back movement of the outer slide rod. The folding mechanism can be realized from fully unfolded to folded to a certain position by controlling the backward movement of the cylindrical pin shaft, and the folding mechanism can be realized from the folded state to fully unfolded by controlling the forward movement of the cylindrical pin shaft. Therefore, in the upstroke of the bat wings, the folding mechanism first goes from fully unfolded to folded, and then from folded to fully unfolded.

During a period of flapping of the bat wings, the wings are fully expanded during the downstroke to ensure the maximum area; during the upstroke, the folding mechanism is first folded and then fully expanded. The locking mechanism just realizes the coupling of the flapping movement and folding movement of the bat wings.

The folding mechanism and the locking mechanism are assembled in the CATIA software, and the folding mechanism is fully expanded and folded as shown in Figure 11 and Figure 12, respectively.

Figure 11 – Fully expanded view of the folding mechanism after assembly of the folding mechanism and the locking mechanism.

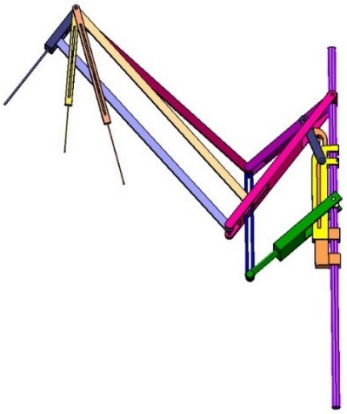

Figure 12 – Fully folded view of the folding mechanism after assembly of the folding mechanism and the locking mechanism.

3.3 Drive mechanism design

It is necessary to design a single-degree-of-freedom drive mechanism, which can drive the entire folding mechanism to flap, and also drive the outer sliding rod of the locking mechanism to move along the right cylindrical fixed rod, that is, to realize the coupling of the flapping movement and the folding movement of the folding mechanism.

In order to realize this function, a gear mechanism is designed, which realizes the coupling of flapping movement and folding movement of the folding mechanism by rotating the gear around its own axis, as shown in Figure 13.

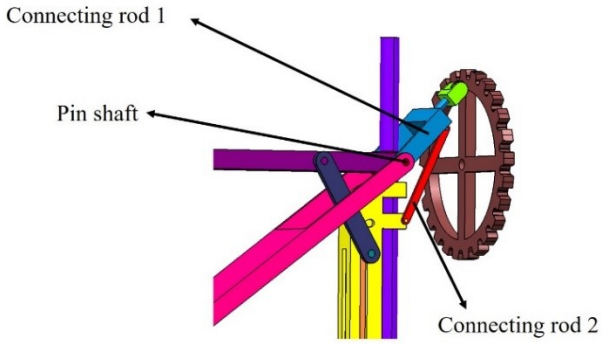

Figure 13 – Single-degree-of-freedom gear drive mechanism.

During the rotation of the gear around its own axis, any point on the circumference of the gear makes a circular motion. The circular motion can be decomposed into horizontal and vertical reciprocating linear motions, and these two reciprocating linear motions can just realize the reciprocating flapping and folding of the folding mechanism.

As shown in Figure 13, the up and down reciprocating movement of the points on the gear circle is mainly realized by the action of the connecting rod 1 to realize the reciprocating rotation of the entire folding mechanism around the cylindrical fixed rod, thereby realizing the up and down reciprocating movement of the entire folding mechanism. The forward and backward reciprocating motion of the points on the gear circle drives the connecting rod 1 to reciprocate around the pin shaft, and then drives the connecting rod 2 to realize the reciprocating and translational movement of the outer sliding rod in the locking mechanism along the cylindrical fixed rod, thereby realizing the reciprocating folding of the folding mechanism. Finally, the flapping movement and the folding movement of the folding mechanism are coupled through the single-degree-of-freedom rotation of the gear.

Assemble the driving mechanism, locking mechanism and folding mechanism in the CATIA software. Figure 14 shows the mechanism diagram of the final folding mechanism at 4 different moments in a flapping cycle.

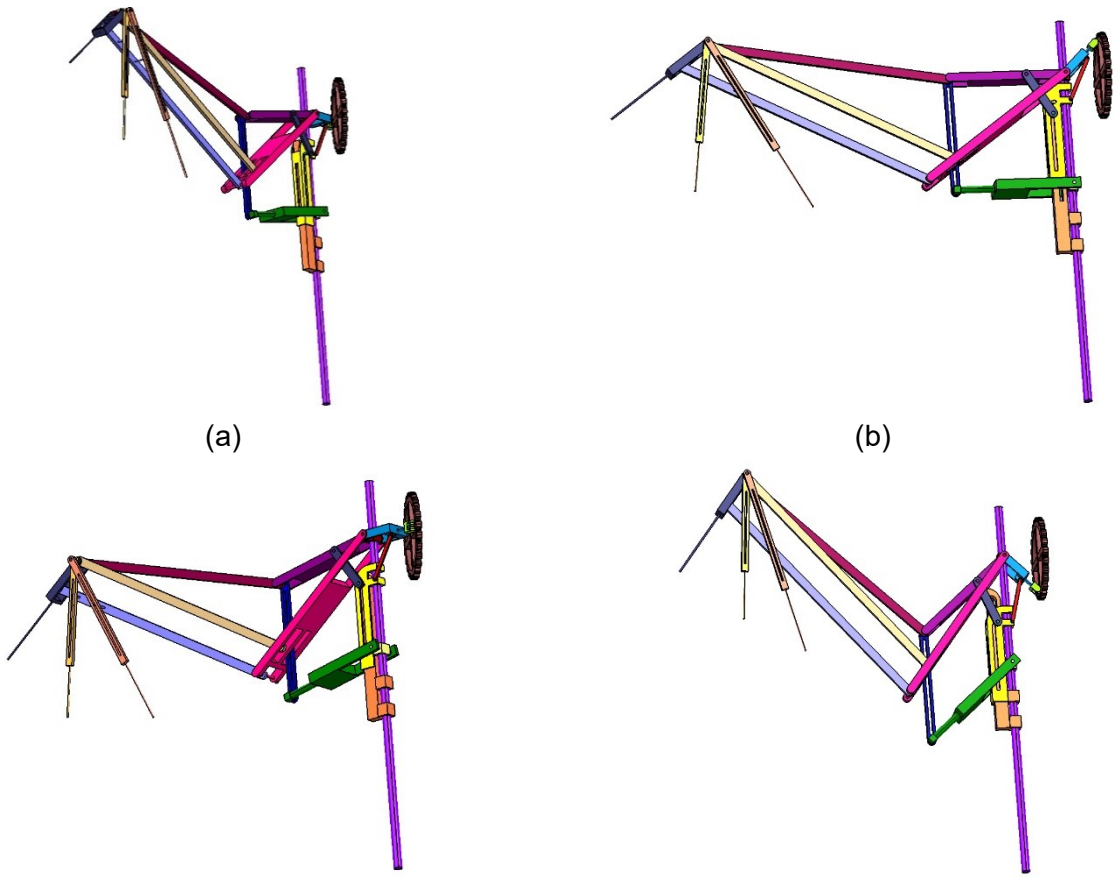

Figure 14 – The final folding mechanism at 4 different moments in a flapping cycle.

4. Numerical Simulation

4.1 Physical model and kinematics

In order to study the influence of the wing folding effect on the aerodynamic performance of the flapping wing, the folded wing is simplified as a rectangular flat plate with chord length c=0.1m, maximum wingspan of 2.5c, and plate thickness 0.02c. As shown in Figure 15, the wing has two degrees of freedom of motion, flapping around the x-axis and folding along the wingspan. According to the design of the bat-like folding mechanism, the wing is fully unfolded on the downstroke, and the wing is first contracted and then unfolded to the initial position on the upstroke. The designed motion law is shown in Figure 16. The red line indicates that the flapping motion is simple harmonic motion. The green line indicates that the wing is fully deployed during the downstroke, and then first retracted to 80% of the maximum wingspan during the upstroke and then fully deployed. For comparison, a wing without retractable wingspan is also simulated, which is called rigid wing in this paper and has a constant wingspan of 2.5c. The blue dash line represents the rigid wing.

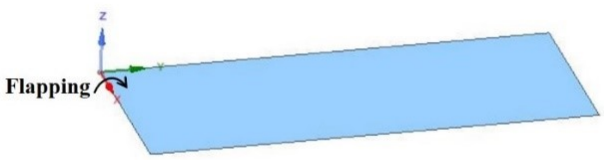

Figure 15 – Rectangular wing model.

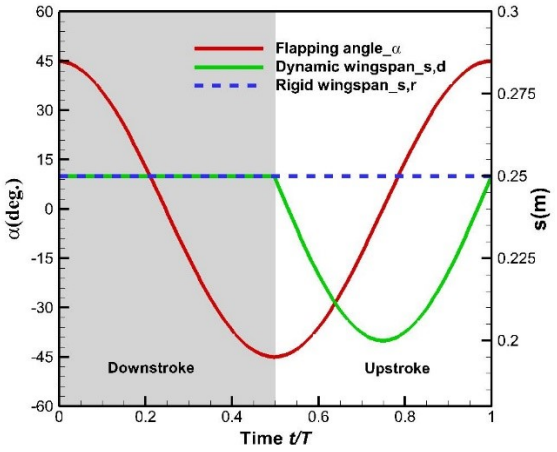

Figure 16 – The law of wing flapping and spanwise contraction.

The law of flapping movement is:

$$\alpha(t) = \alpha_m \cos(2\pi ft) \tag{1}$$

Define the motion law of the folded wingspan factor as:

$$LF(t) = 1 + 0.2 * \sin(2\pi ft) \tag{2}$$

The motion law of the folded wingspan is as follows:

$$S(t) = \begin{cases} S_m & downstroke \\ S_m \bullet LF(t) & upstroke \end{cases} \tag{3}$$

where, α_m is the flapping amplitude, which is equal to 45deg, f is the flapping frequency, which is equal to 4Hz, and S_m is the rigid wingspan, which is equal to 2.5c.

The wing at different times of the downstroke and the upstroke is shown in Figure 17.

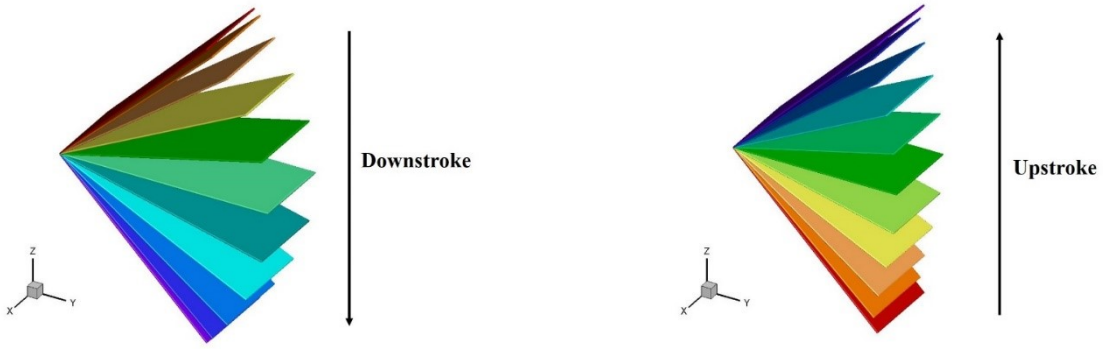

(a) (b)

Figure 17 – Wing at different times of downstroke(a) and upstroke(b).

4.2 Parameters settings

The fluid velocity is U_∞=5m/s, the wing angle of attack is 5deg, according to the Reynolds number calculation formula:

$$\mathrm{Re} = \frac{U_\infty \cdot c}{\nu} \tag{4}$$

where ν is fluid kinematic viscosity, U_∞ reference velocity, c reference mean chord length.

The Reynolds number $\mathrm{Re}=3.4\times10^4$ can be calculated.

Since the wingspan of the folding wing changes during the movement, the wing area is also constantly changing. In order to remove the influence of the wing area, the lift coefficient Cl_t and the thrust coefficient Ct_t which are dimensionless from the instantaneous wing area are introduced:

$$\mathrm{Cl}_t(t)=\frac{L(t)}{q_\infty S(t)} \tag{5}$$

$$\mathrm{Ct}_t(t)=\frac{T(t)}{q_\infty S(t)} \tag{6}$$

where $L(t)$ is the instantaneous lift, q_∞ is the dynamic pressure, $S(t)$ is the instantaneous wing area, and $T(t)$ is the instantaneous thrust.

Through the simulation calculation of flapping wing with folding movement, as well as pure flapping wing, the aerodynamic changes of the two motions are obtained, and then the influence of spanwise folding motion on aerodynamic forces is compared and analyzed.

4.3 Calculation method and mesh

Use Fluent commercial software to solve the Navier-Stokes equation, choose the Reynolds-Averaged Navier-Stokes method to solve, and use the Shear Stress Transport k-ω turbulence model. User defined function is used to control the flapping and folding movement of the wing. An overset mesh is used for calculation, the calculation domain size is 62c×42c×21c, the background mesh is structured mesh, and the component mesh is tetrahedral unstructured mesh. The calculation time step is T/200. The computational mesh is shown in Figure 18.

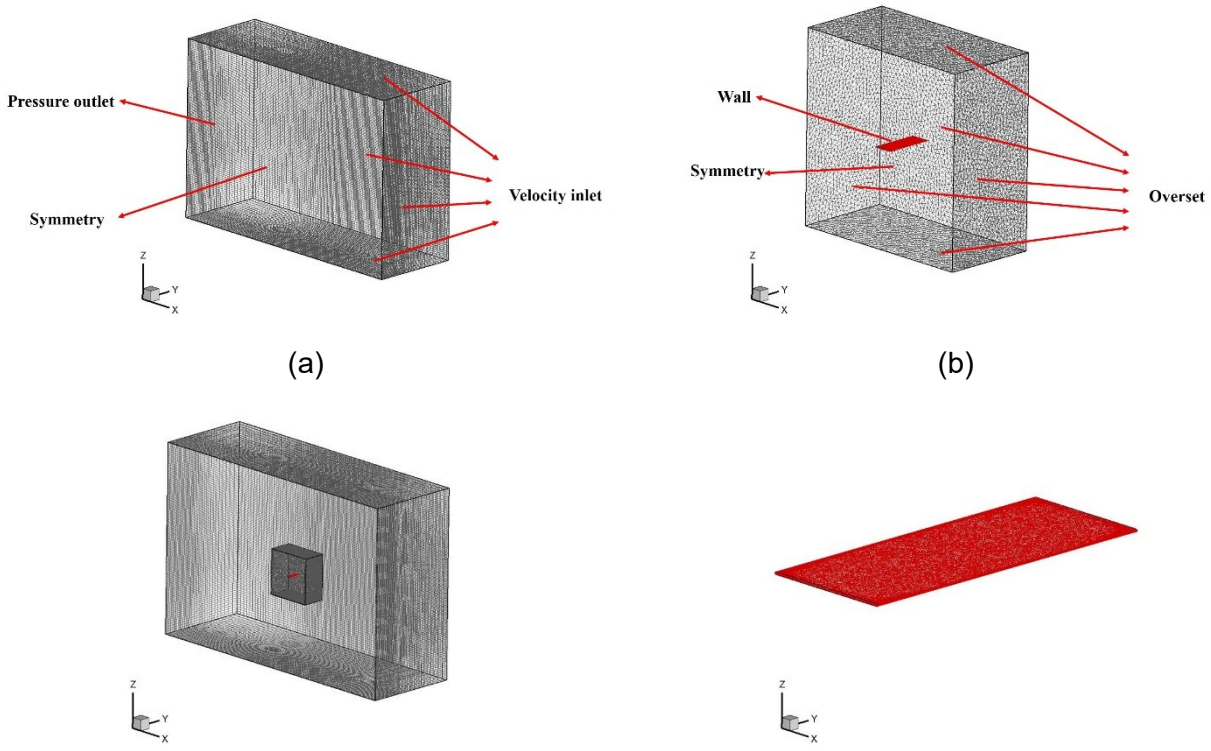

Figure 18 – The mesh used in the current study: (a) the background mesh, (b) the component mesh, (c) the total mesh system, and (d) the surface mesh of the wing.

4.4 Results and discussion

After three cycles of calculation, the changes of aerodynamic force tend to be stable, and the calculation results of the fourth cycle are extracted for comparative analysis. The lift coefficients are shown in Figure 19(a). The overall change of the lift coefficient curves of wing are the same under the two motion laws. The lift coefficient of the downstroke is relatively large and reaches its peak at the middle of the downstroke. The lift coefficient of the upstroke becomes smaller, and negative lift appears, reaching the minimum value at the middle of the upstroke. Since the area of the retractable wing remains constant during the downstroke, the result is the same as that of the rigid wing. During the upstroke, due to the reduced wing area, the negative lift of the retractable wing is reduced, thereby increasing the average lift.

The curves of thrust coefficients are shown in Figure 19(b). It can be seen that drag will be generated before and after the flapping reversal, and thrust will be generated during rest of time. During the downstroke, the retractable wing thrust curve is the same as that of the rigid wing. During the upstroke, the peak thrust will decrease, this is due to the reduced wing area. It can be seen that the retractable wing increases lift at the expense of reduced thrust during the upstroke.

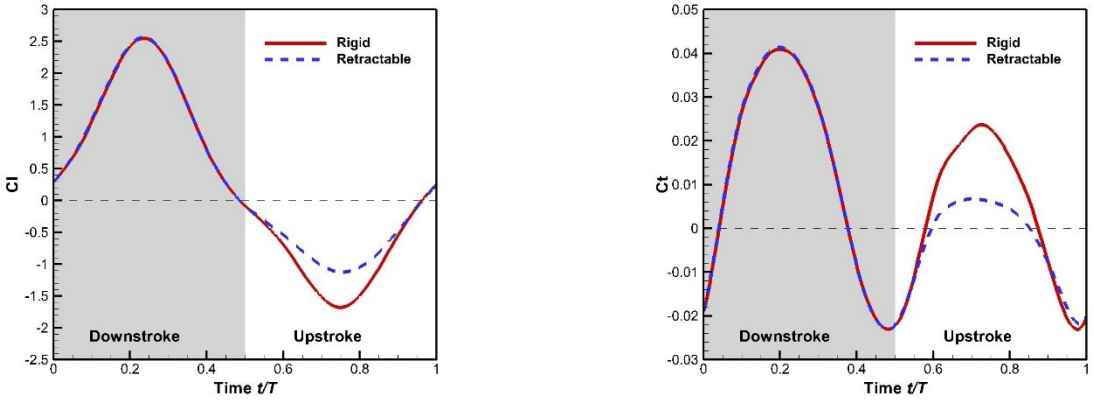

(a) (b)

Figure 19 – Curves of lift coefficient and thrust coefficient of retractable wing and rigid wing.

5. conclusion

In this paper, by observing the movement of the bat wings in flight, a folding wing mechanism is proposed, which keeps the wings fully expanded during the downstroke, and retracts and then expands during the upstroke. By simplifying the folding wing to a flat wing for numerical calculation, comparing the lift and thrust of the wing with and without spanwise contraction, it is found that the lift and thrust are the same during the downstroke because the area of the retractable wing remains unchanged. During the upstroke, due to the reduced area of the retractable wing, the negative lift is reduced, thereby increasing the average lift, but at the same time the thrust is also reduced.

6. Contact Author Email Address

mailto: yb@mail.nwpu.edu.cn

7. Copyright Statement

The authors confirm that they, and/or their company or organization, hold copyright on all of the original material included in this paper. The authors also confirm that they have obtained permission, from the copyright holder of any third party material included in this paper, to publish it as part of their paper. The authors confirm that they give permission, or have obtained permission from the copyright holder of this paper, for the publication and distribution of this paper as part of the ICAS proceedings or as individual off-prints from the proceedings.

8. Acknowledgments

This study was supported by the National Natural Science Foundation of China (11872314) and the Key R&D Program in Shaanxi Province of China (2020GY-154).

References

[1] Pornsin-Sirirak T N, Tai Y C, Ho C M, et al. Microbat: A Palm-Sized Electrically Powered Ornithopter[J]. *proceedings of the nasa/jpl workshop on biomorphic robotics*, 2001.
[2] Pornsin-Sirirak T N, Tai Y C, Nassef H, et al. Titanium-alloy MEMS wing technology for a micro aerial vehicle application[J]. *Sensors & Actuators A Physical*, 2001, 89(1-2): 95-103.
[3] Chung S J, Dorothy M. Neurobiologically Inspired Control of Engineered Flapping Flight[J]. *Journal of Guidance Control and Dynamics*, 2009, 33(2): 440-453.
[4] Ramezani A, Shi X, Chung S J, et al. Modeling and Nonlinear Flight Controller Synthesis of a Bat-Inspired Micro Aerial Vehicle[C]. *Aiaa Guidance, Navigation, & Control Conference*, 2016.
[5] Breuer K, Schunk C, Bahlman J, et al. Measurement of the wake behind a bat-like flapper and the influence of the flapping frequency on lift generation[C]. *6th AIAA Theoretical Fluid Mechanics Conference*, 2011.
[6] Bahlman J W, Swartz S M, Breuer K S. Design and characterization of a multi-articulated robotic bat wing[J]. *Bioinspiration & Biomimetics*, 2013, 8(1): 016009.
[7] Bahlman J W, Swartz S M, Breuer K S. How wing kinematics affect power requirements and aerodynamic force production in a robotic bat wing[J]. *Bioinspiration & Biomimetics*, 2014, 9(2): 025008.
[8] Chen P, Joshi S, Swartz S M, et al. Bat inspired flapping flight[C]. *22nd AIAA/ASME/AHS Adaptive Structures Conference - SciTech Forum and Exposition 2014*, January 13, 2014 - January 17, 2014, 2014: AIRBUS; BOEING; DUNMORE; Lockheed Martin.
[9] Koekkoek G, Muijres F T, Johansson L C, et al. Stroke plane angle controls leading edge vortex in a bat-inspired flapper[J]. *Comptes rendus - Mécanique*, 2012, 340(1-2): 95-106.
[10] Colorado J, Barrientos A, Rossi C. Biomechanics of morphing wings in a Bat-robot actuated by SMA muscles[C]. *The International Workshop on bio-inspired robots*, 2011.
[11] Colorado J, Barrientos A, Rossi C, et al. Biomechanics of smart wings in a bat robot: morphing wings using SMA actuators[J]. *Bioinspiration & Biomimetics*, 2012, 7(3): 16.
[12] Colorado J, Barrientos A, Rossi C, et al. Inertial attitude control of a bat-like morphing-wing air vehicle (vol 8, 016001, 2013)[J]. *Bioinspiration & Biomimetics*, 2013, 8(1): 18.
[13] Colorado J, Rossi C, Barrientos A, et al. The Influence of Bat Wings For Producing Efficient Net Body Forces in Bio-inspired Flapping Robots[J]. *IEEE*, 2014: 528-532.
[14] Colorado J, Rossi C, Zhang C, et al. Towards efficient flight: insights on proper morphing-wing modulation in a bat-like robot[J]. *Advanced Robotics*, 2015, 29(24): 1599-1610.